ACS APPLIED MATERIALS & INTERFACES

Research Article

www.acsami.org

Facile Solvothermal Synthesis of Porous Cubic Cu Microparticles as Copper Catalysts for Rochow Reaction

Zailei Zhang,[†,‡] Hongwei Che,[†] Yingli Wang,[†] Xilin She,[‡] Jin Sun,[‡] Poernomo Gunawan,[§] Ziyi Zhong,[§] and Fabing Su*[,†]

[†] State Key Laboratory of Multiphase Complex Systems, Institute of Process Engineering, Chinese Academy of Sciences, Beijing, China 100190

[‡] College of Chemical and Environmental Engineering, Qingdao University, Qingdao, China 266071

[§] Institute of Chemical Engineering and Sciences, A*star, 1 Pesek Road, Jurong Island, Singapore 627833

ABSTRACT: Porous cubic Cu microparticles were synthesized by a facile solvothermal method using $Cu(CH_3COO)_2 \cdot H_2O$ as the Cu precursor and NaOH in a solution containing ethanol, ethylene glycol, and water. The synthesis conditions were investigated and a growth process of porous cubic Cu microparticles was proposed. The catalytic properties of the porous Cu microparticles as model copper catalysts for Rochow reaction were explored. The samples were characterized by X-ray diffraction, scanning electron microscopy, transmission electron microscopy, thermogravimetric analysis, temperature-programmed reduction, and nitrogen adsorption. It was found that the morphology and structure of the porous cubic Cu microparticles are highly dependent on the reaction time and temperature as well as on the amount of reactants added. Compared to the commercial Cu microparticles with irregular morphology and dense internal structure, porous cubic Cu microparticles show much higher dimethyldichlorosilane selectivity and Si conversion via Rochow reaction, which are attributed to the enhanced formation of active Cu_xSi phase and gas transportation in the presence of the pore system within microparticles, demonstrating the significance of the pore structure of the copper catalysts in catalytic reactions of organosilane synthesis.

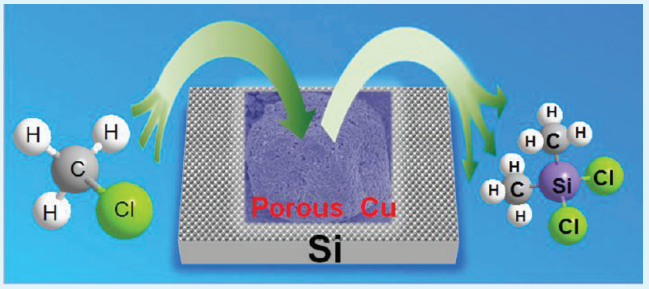

KEYWORDS: *porous cubic Cu microparticles, solvothermal method, copper catalysts, Rochow reaction*

1. INTRODUCTION

Recently, the fabrication of metals, with specific structural features, has been of great interest because of the impact of these features in areas of basic scientific research and potential applications.[1−4] Many porous metals such as Ag,[5] Zn,[6] Ni,[7] Au,[8] Pt,[9] and Cu[10] have been prepared by electrochemical method,[11] chemical etching method,[12] modified polyol method,[9] and template-free route.[13] These porous metals can be used in optical adsorption,[13] enhanced Raman scattering,[8] biosensor,[12] catalysis,[9] lithium-ion batteries,[14,15] and fuel cell.[7,16] Among these metals, structured metallic Cu has attracted intense attention because of its wide applications in electronics,[17] catalysis,[18] CO adsorption,[19] NO adsorption,[20] conduction,[21,22] and optical devices.[23] The synthesized Cu structures include Cu nanowires,[24] Cu nanodisks,[25] cubic Cu mesocrystals,[26] sheet-like Cu dendrites,[27] Cu nanorods,[28] dendritic Cu nanostructures,[29] Cu nanocrystals,[30] and shape-controlled Cu colloids.[31] Porous hierarchical copper dendrites were synthesized by a facile hydrothermal treatment of copper-glycine complex in solution.[10] Cao and co-workers prepared cubic Cu mesocrystals by a solvothermal reaction.[26] Hollow Cu nano/microstructures were prepared by reduction of $CuSO_4$ with glucose by using a mild hydrothermal process.[32] These synthesis approaches often involve electroless deposition,[29] multiple deposition parameter control,[33] high temperatures and pressures and long reaction times,[28] toxic reducing agents,[24] large excess of reducing agents,[25] and template surfactants.[32]

Since Rochow discovered the direct synthesis route to produce methylchlorosilanes (MCSs) using Si to react with chloromethane (MeCl) (named Rochow reaction) in the 1940s,[34] metallic Cu[35] and Cu compounds such as Cu_2O,[36] CuO,[37,38] $Cu−Cu_2O−CuO$ composite,[39] and $CuCl_2$[40] have been found as active copper catalysts for this reaction. The copper-based catalysts used always have dense structures, irregular morphologies and micrometer sizes.[41,42] Because porous catalysts are often able to enhance catalytic performances[43−45] and the presence of a large number of pores within these micrometric copper particles could save the catalyst cost for industry application, it is desired to develop novel porous copper-based catalysts for MCS synthesis.

In our previous work,[36,38] we found the improved catalytic properties of the mesoporous Cu_2O and flowerlike CuO

Received: November 9, 2011
Accepted: February 24, 2012
Published: February 24, 2012

microspheres as model copper-based catalysts for dimethyldichlorosilane synthesis via the Rochow reaction. Herein, we present a simple method to prepare porous Cu microparticles with a cubic morphology as model copper catalysts for Rochow reaction. The porous cubic Cu microparticles are synthesized by a solvothermal method in ethanol, ethylene glycol, and water systems under alkaline condition. The microstructure of the porous Cu particles can be controlled by adjusting the synthesis condition. Compared with the commercial dense Cu microparticles, these porous cubic Cu microparticles show much higher dimethyldichlorosilane selectivity and Si conversion, demonstrating the significance of the pores within the Cu catalysts. Our work would be helpful for developing novel porous copper catalysts and understanding the catalytic mechanism. The present study also adds a new example of porous metals and would be helpful for us to understand the formation mechanism of other porous metals.

2. EXPERIMENTAL SECTION

2.1. Synthesis of Materials. The porous cubic Cu microparticles were synthesized using a solvothermal method.[26] The synthesis scheme is shown in Figure 1. To optimize the synthesis condition and investigate the product formation mechanism, the synthesis parameters such as the reaction temperature, time, and reactants amount were varied while keeping all other experimental parameters constant (see Table 1). In a typical synthesis (e.g., sample S3 in Table 1), 1.00 g of copper acetate ($Cu(CH_3COO)_2{\cdot}H_2O$, A.R., Sinopharm Chemical Reagent Co., Ltd., China) was dissolved in 10.0 mL of deionized water, which was then mixed with 50.0 mL absolute alcohol (CH_3CH_2OH, A.R., Sinopharm Chemical Reagent Co., Ltd., China) and 20.0 mL ethylene glycol (EG) ($C_2H_6O_2$, A.R., Sinopharm Chemical Reagent Co., Ltd., China) to form a solution in a beaker, followed by adding 1.40 g of sodium hydroxide (NaOH, A.R., Sinopharm Chemical Reagent Co., Ltd., China). After being stirred for 10 min, the solution was transferred into 100 mL of Teflon-lined stainless-steel autoclave. The autoclave was sealed and maintained at 160 °C for 10 h, and then cooled down to room temperature. The resulting precipitate was collected by centrifugation, washed with distilled water and pure ethanol, and finally dried in a vacuum at 60 °C for 8 h. Ten milliliters of deionized water, 50.0 mL of absolute alcohol, and 20.0 mL of EG were constant for all sample synthesis.

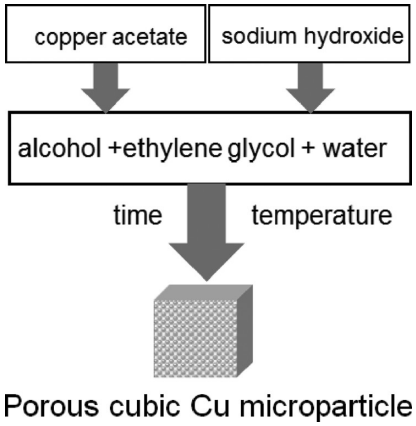

Figure 1. Preparation scheme of porous Cu microparticles.

2.2. Characterization of Materials. X-ray diffraction (XRD) patterns were recorded on a PANalytical X'Pert PRO MPD using the Kα radiation of Cu (λ = 1.5418 Å) and checked with the card number of Joint Committee on Powder Diffraction Standards (JCPDS). The crystallite size was calculated using the Debye–Scherrer equation.[46,47] The microscopic feature of the samples was observed by field-emission scanning electron microscopy (SEM) (JSM-6700F, JEOL, Tokyo, Japan) with energy-dispersive spectroscopy (EDS) and transmission electron microscopy (TEM) (JEM-2010F, JEOL, Tokyo, Japan). Adsorption–desorption isotherms of N_2 at 77 K were measured using a surface area and pore size analyzer (NOVA 3200e, Quantachrome). Prior to the measurement, the sample was degassed at 200 °C for 4 h under vacuum. The specific surface area was determined according to the Brunauer–Emmett–Teller (BET)[48] method in the relative pressure range of 0.05–0.2. The pore size distribution was calculated by the Barrett–Joyner–Halenda (BJH) method using the adsorption isotherm branch.[49] Thermal gravimetric (TG) analysis was carried out on an EXSTAR TG/DTA 6300 (Seiko Instruments, Japan) with a heating rate of 10 °C/min in air (200 mL/min). Temperature programmed reduction (TPR) measurements were carried out on Automated chemisorption analyzer (ChemBET pulsar TPR/TPD, Quantachrome). Upon loading of 0.10 g of Cu microparticles into a quartz U-tube, the sample was degassed at 200 °C for 30 min under helium. When the temperature dropped to 20 °C, the gas was changed to 9.9% H_2/Ar. Finally, the sample was heated from 20 to 800 °C with 10 °C/min in 9.9% H_2/Ar with a gas flow of 30 mL/min.

Table 1. Synthesis Conditions Used in the Preparation of Porous Cu Microparticles

sample	copper acetate (g)	sodium hydroxide (g)	reaction T (°C)	reaction t (h)
S1	1.00	1.40	160	3
S2	1.00	1.40	160	6
S3	1.00	1.40	160	10
S4	1.00	1.40	160	16
S5	1.00	1.40	160	24
S6	1.00	1.40	160	48
S7	0.20	0.28	160	10
S8	0.50	0.70	160	10
S9	1.50	2.10	160	10
S10	2.00	2.80	160	10
S11	4.00	5.60	160	10
S12	1.00	1.40	120	10
S13	1.00	1.40	140	10
S14	1.00	1.40	180	10

2.3. Characterization of Catalytic Behavior. The evaluation of the catalyst was carried out with a typical MCS lab fixed-bed reactor as reported.[37] Ten grams of Si powder (20–50 mesh, provided by Jiangsu Hongda New Material Co., Ltd., China, the contents of impurity are compiled in Table 2) and 1.0 g of porous Cu microparticles together with 0.1 g of Zinc (Zn, A.R., Sinopharm Chemical Reagent Co., Ltd., China) used as a promoter were homogeneously ground in mortar for 10 min to form a contact mass, which was then loaded in the glass reactor. The reactor system was purged with purified N_2 for 0.5 h followed by a heating to 325 °C within 1 h under N_2 flow rate of 25 mL/min. Subsequently, N_2 was

Table 2. Contents of the Impurity within Reactant Si Particles[a]

impurities	content (wt %)
Fe	0.21
Al	0.15
Ca	0.12
Mg	0.003
Cu	0.004
Pb	<0.001
Ti	<0.002
Mn	<0.001

[a]Data were provided by the company.

turned off and MeCl gas with a flow rate of 25 mL/min was introduced into the reactor to react with Si at 325 °C. After 24 h, the reaction was stopped. The gaseous product was condensed with a circulator bath controlled at 5 °C by a programmable thermal circulator (GDH series, Ningbo xinzhi biological technology Co., LTD, China). The waste contact mass (solid residue after reaction) containing unreacted Si powder and copper catalysts was weighed for calculating the Si conversion. The condensed liquid phase was analyzed with gas chromatography (GC) System (Agilent Technologies GC-7890A. Rochow reaction is expressed in formula 1 as follows

$$\mathrm{Si + MeCl} \xrightarrow[\text{300-350 °C}]{\text{copper catalyst}} \begin{matrix}(CH_3)_3SiCl\\(CH_3)_2SiCl_2\\CH_3SiCl_3\\CH_3HSiCl_2\\(CH_3)_2HSiCl\\\text{other low boilers}\\\text{residue}\end{matrix} \quad (1)$$

In this reaction, the product mainly consists of methyltricholorsilane (CH_3SiCl_3, M1), dimethyldichlorosilane ($(CH_3)_2SiCl_2$, M2), and trimethylchlorosilane ($(CH_3)_3SiCl$, M3), which are normally accounted for more than 95 wt % of the total reaction products.[50] For the calculation of the Si conversion, because the weight of Cu (and Zn) keeps unchanged after reaction, we can know the total amount of Si+Cu before reaction, subtracting the weight of solid residue (Si+Cu) after reaction to get the Si conversion. Among the three silane products, M2 is the most desired monomer, which is used to synthesize organosilicon products in industry. Thus, for simplifying the calculation, other trace products and the change of catalyst will be ignored, and Mi (i = 1, 2, 3) selectivity and Si conversion can be derived from the following formulas:

$$\text{selectivity of M}i\ (S_{\mathrm{M}i}) = \frac{\text{mole}_{\mathrm{M}i}}{\sum_{i=1}^{3}\text{mole}_{\mathrm{M}i}} \times 100\% (i = 1, 2, 3) \quad (2)$$

$$\text{conversion of Si}(C_{\mathrm{Si}}) = \frac{\text{weight}_{\text{contact mass before reaction}} - \text{weight}_{\text{contact mass after reaction}}}{\text{weight}_{\text{Si before reaction}}} \times 100\% \quad (3)$$

The commercial dense Cu microparticles (Sinopharm Chemical Reagent Co., Ltd., China) was employed for a comparison. Figure

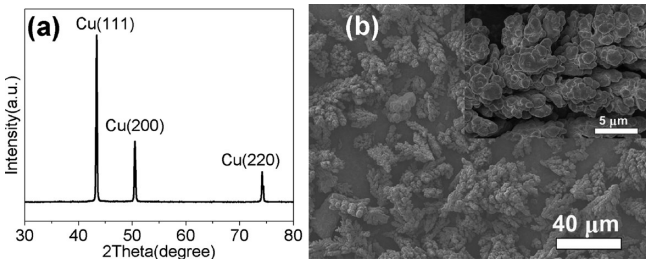

Figure 2. (a) XRD pattern and (b) SEM image of commercial Cu microparticles (insets is its high-magnification image).

2a shows their XRD pattern, indicating the phase-pure Cu. Figure 2b presents their SEM image showing branch-like morphology with wide particle size distribution of 5−40 μm.

3. RESULTS AND DISCUSSION

Figure 3a shows the XRD patterns of the porous cubic Cu microparticles prepared (sample S3 in Table 1). The diffraction peaks at 2θ values of 43.3, 50.5, and 74.2° correspond to the lattice plane of (111), (200), and (220), respectively, indicating the formation of pure Cu phase with cubic symmetry (JCPDS

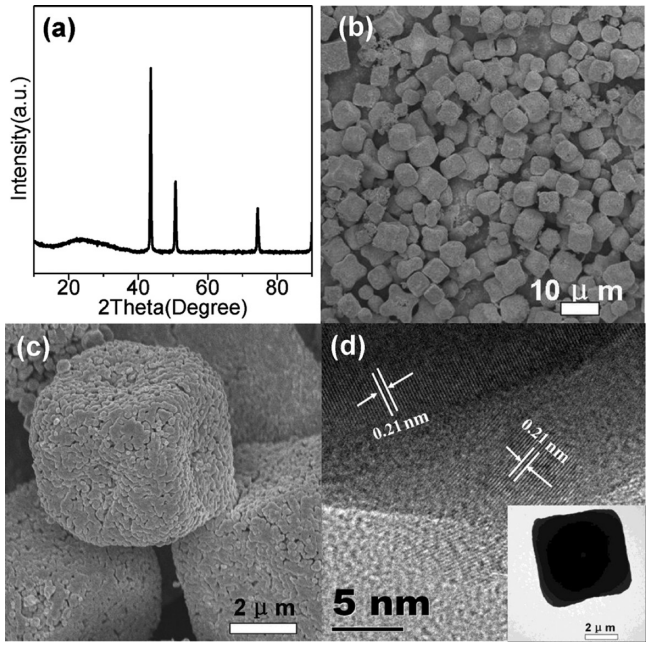

Figure 3. (a) XRD pattern, (b, c) SEM image, and (d) HRTEM image of the porous cubic Cu microparticles, (inset is low magnification) (sample S3 in Table 1).

No. 01−070−3039). Figure 3b shows the SEM image of the porous Cu microparticles with a cubic morphology. Their size is about 3−6 μm. A single Cu microparticle (Figure 3c) reveals the presence of a large number of pores on its surface. Figure 3d shows a HRTEM image taken at the edge of a Cu microparticle, indicating polycrystalline Cu with a spacing distance of 0.21 nm, which corresponds to the distance of the (111) plane of the metallic Cu cubic symmetry. Inset of Figure 3d further exhibits the cubic morphology. BET surface area of S3 sample was measured to be 5.7 m^2/g, further demonstrating the presence of pores within the S3 sample. The effects of synthesis conditions such as reaction time and temperature, as well as reactant amounts added on the pore structure and morphology of Cu microparticles were investigated and their formation mechanism was proposed further.

3.1. Effects of Reaction Time. Figure 4a shows the XRD patterns of the samples obtained at different reaction times. At a short reaction time for Cu product synthesis (3 h, sample S1), the diffraction peaks at 2θ values of 36.5, 42.2, 61.3, and 73.3° correspond to the lattice planes of (111), (200), (220), and (311) respectively of cubic Cu_2O (JCPDS No. 03−0892), thus it formed pure Cu_2O. When the reaction time is prolonged to 6 h, besides the Cu_2O diffraction peaks, some other peaks at 2θ values of 43.3, 50.5, and 74.2° are also observed, which correspond to the lattice planes of (111), (200), and (220) of the cubic symmetry Cu (JCPDS No. 01−070−3039), suggesting S2 sample is composed of a mixture of Cu_2O and Cu phases. When the synthesis time is extended to 10 h (S3), 16 h (S4), 24 h (S5), and 48 h (S6) respectively, all of the obtained samples are pure metal Cu materials. The average Cu_2O crystal size for S1 is calculated to be about 52 nm, and Cu crystal size is around 43 nm for S3, S4, S5 and S6 samples, indicating the average crystal size of Cu_2O is larger than that of Cu. Figure 4b shows the SEM image of sample S1. It can be seen that S1 possesses a cubic morphology with a microparticle size of 4−5 μm and no pores are observed on its surface. As the

dx.doi.org/10.1021/am3002605 | ACS Appl. Mater. Interfaces 2012, 4, 1295−1302

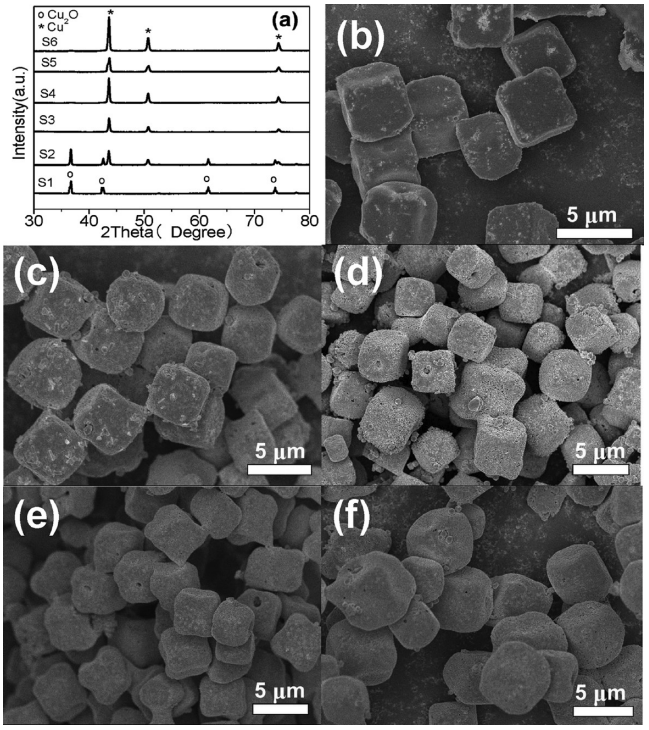

Figure 4. (a) XRD patterns and SEM images of products obtained at different reaction times: (b) 3 h (S1), (c) 6 h (S2), (d) 10 h (S3), (e) 16 h (S4), and (f) 24 h (S5).

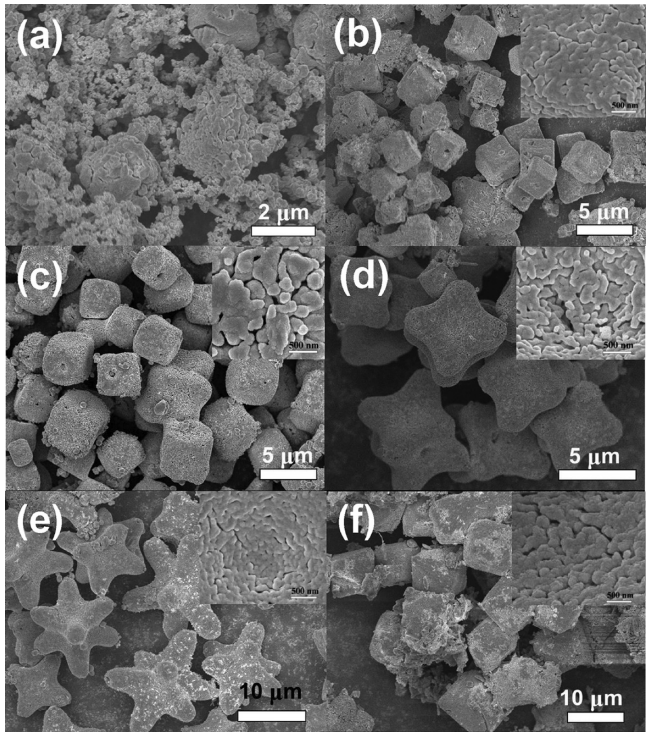

Figure 5. SEM images of porous Cu obtained with different amounts of copper acetate and sodium hydroxide: (a) 0.20 and 0.28 g (S7), (b) 0.50 and 0.70 g (S8), (c) 1.00 and 1.40 g (S3), (d) 1.50 and 2.10 g (S9), (e) 2.00 and 2.80 g (S10), and (f) 4.00 and 5.60 g (S11) (insets are high-magnification images of the each sample surface).

reaction time is prolonged to 6 h for S2, some pores are created on its surface as shown in Figure 4c, but there is no obvious change in the microparticle size. For sample S3 prepared with a reaction time of 10 h, a large number of pores are found as shown in Figure 4d, demonstrating the formation of porous cubic Cu microparticles with a particle size of 3−6 μm, which are also observed for samples S4 (Figure 4e), S5 (Figure 4f), and S6 (not shown here). Therefore, a 10 h reaction time is enough to obtain porous cubic Cu microparticles.

3.2. Effects of Reactant Amounts. XRD patterns of samples S3 and S7−S11 prepared with different amounts of copper acetate (m1) and sodium hydroxide (m2) indicate the formation of metallic Cu with cubic symmetry (not shown here). Figure 5a displays the SEM image of sample S7. It can be seen that S7 comprises of both nanoparticles and microparticles. As the reactant amounts were increased ($m1$ = 0.50 g and $m2$ = 0.70 g), more pores were developed (sample S8) as shown in Figure 5b, which possesses a cubic morphology and a microparticle size of 4−5 μm. For sample S3, which was prepared with $m1$ = 1.00 g and $m2$ = 1.40 g, a large number of pores are observed in Figure 5c, demonstrating the formation of porous cubic Cu microparticles with a size of 3−6 μm. With further increase in the reactant amounts to $m1$ = 1.5 g and $m2$ = 2.1 g, the obtained S9 sample consists of uniform and porous octagonal Cu particles in the size range of 3−7 μm, with the creation of numerous pores on its surface as shown in Figure 5d. Samples S10 (Figure 5e) and S11 (Figure 5f) exhibit a similar pore structure on their surfaces. With $m1$ = 2.00 g and $m2$ = 2.80 g (S10), it resulted in relatively uniform porous octagonal Cu with a larger size of 7−12 μm as shown in Figure 5e, whereas with $m1$ = 4.00 g and $m2$ = 5.60 g (S11), it formed nonuniform porous octahedral Cu with a size of 8−10 μm as shown in Figure 5f. Overall, the product yield is higher than 95%.

3.3. Effects of Reaction Temperature. Figure 6a shows XRD patterns of the products formed at different reaction temperatures. When the reaction was conducted at 120 °C (S12) and 140 °C (S13), respectively, for 10 h, four diffraction peaks at 2θ values of 36.5, 42.2, 61.3, and 73.3° are observed, which correspond to the (111), (200), (220), and (311) lattice planes of pure Cu_2O with cubic symmetry (JCPDS No. 03−0892). Further increasing the reaction temperature to 160 °C (S3), and 180 °C (S14), the peaks appear at 2θ values of 43.3, 50.5, and 74.2°, which correspond to the lattice planes of (111), (200), and (220) of the cubic symmetry Cu (JCPDS No. 01−070−3039), suggesting the formation of pure Cu. Figure 6b shows the SEM image of the sample S12 obtained at 120 °C. It is observed that S12 exhibits nonuniform cubic and octagonal Cu_2O morphology with particle size of 5−8 μm. Figure 6c displays the SEM image of the sample obtained at 140 °C (S13), which also exhibits a nonuniform cubic and octagonal Cu_2O morphology with a size of 6−9 μm. The high-magnification images b and c in Figure 6 show that the obtained Cu_2O surface is nonporous. Further increasing the reaction temperature to 160 °C (S3) results in the formation of porous cubic Cu with relatively uniform morphology as shown in Figure 6d, of which particle size is about 3−6 μm. At 180 °C, sample S14 formed nonuniform porous Cu with a size of about 3−7 μm (Figure 6e). However, high-magnification images d and e in Figure 6 prove the formation of porous Cu microparticles. As comparison, SEM image of the commercial irregular Cu particles is also presented in Figure 6f and it exhibits nonporous branchlike morphology with wide particle size distribution of 5−40 μm.

3.4. Proposed Formation Mechanism. The possible chemical reactions occurred in the system are expressed in

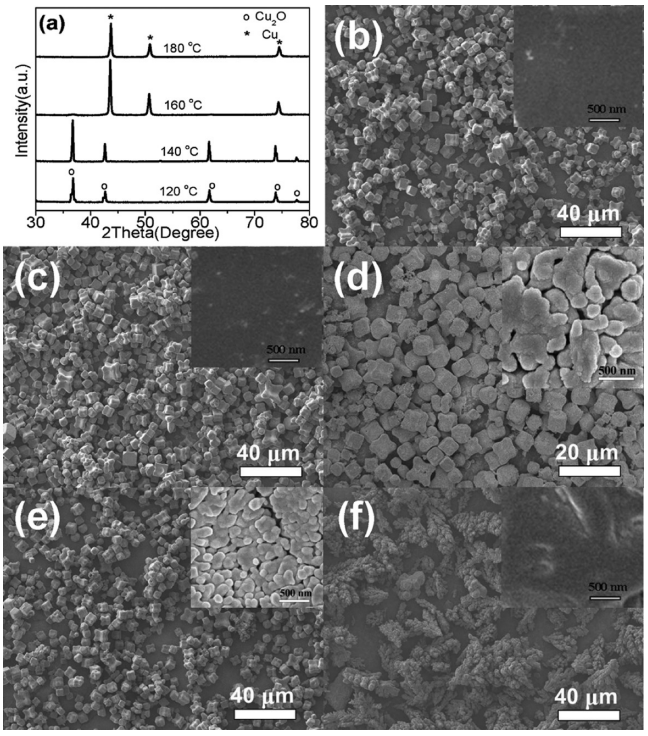

Figure 6. (a) XRD patterns of different products formed at different reaction temperature, SEM images of Cu obtained at (b) 120 °C (S12), (c) 140 °C (S13), (d) 160 °C (S3), (e) 180 °C (S14), and (f) commercial Cu.

equations 1−5. In EG solution, after adding copper precursor, it was observed that the color of the solution was changed from blue to green, suggesting Cu^{2+} ions interact with EG molecules to form a relatively stable $[Cu(II)EG]^{2+}$ complex (eq 1).[51] Then, in the presence of water, the complex could convert into $Cu(OH)_2$ precipitate because the stability constant of the complex is smaller than that of $Cu(OH)_2$ at a high temperature (eq 2).[52] During the reaction, the acetaldehyde molecules formed by the dehydration of EG in the presence of NaOH (eq 3)[53] reduce the $Cu(OH)_2$ precipitates to Cu_2O particles at a relatively high temperature and the autogenerated vapor pressure in closed system (eq 4),[52] which assemble to cubic Cu_2O microparticles. The as-formed unstable Cu_2O particles were further reduced by acetaldehyde molecules to create porous Cu microparticles (eq 5).[51] Figure 7a−c show the

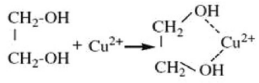

(1)

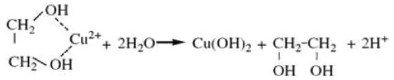

(2)

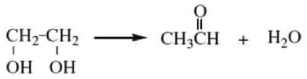

(3)

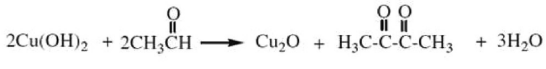

(4)

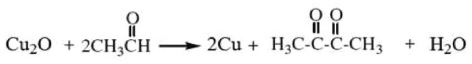

(5)

evolution of cubic Cu_2O (S1) to cubic Cu_2O−Cu composite (S2) and eventually porous cubic Cu (S3), which are confirmed by the XRD analysis (Figure 4a). The EDS analysis of S2 (not shown here) demonstrates that the product was made of Cu and O only with an atomic ratio of approximate 3:1, also proving that the product is Cu_2O−Cu composite. As the particle surface of Figure 7b is of porous structure, which is similar to that of Figure 7c (porous Cu), the surface component should be Cu, whereas the core should be Cu_2O. This is reasonable as the outer surface species will first contact with reductant molecules. On the basis of the above observation, the formation process of the porous cubic Cu is proposed as depicted in Figure 7d, which is a well-assisted two-stage growth model. At the first stage, the copper acetate and sodium hydroxide were reduced by acetaldehyde to form Cu_2O nanoparticles, followed by the self-assembly of Cu_2O nanoparticles to form dense cubic Cu_2O at an appropriate temperature. At the second stage, the initially formed dense cubic Cu_2O were further gradually reduced by acetaldehyde layer by layer to form Cu surface/Cu_2O core until pure porous cubic Cu was formed. EG in this process not only acted as a solvent and reducing agent but also as a structure-directing agent for the formation of porous structure.[54]

3.5. Catalyst Evaluation. Figure 8a presents the TG curves of porous Cu (S3, S9, and S10) and commercial Cu particles in air. The oxidation of porous Cu occurred at about 150 °C and completed at about 500 °C. In contrast, the oxidation for commercial Cu occurred at higher temperature range of 200−700 °C. The complete oxidation temperature of porous Cu was found to be 200 °C lower than that of commercial Cu, suggesting that porous Cu was much more facile to be oxidized than the commercial Cu in air due to the presence of porous structure. The weight of S3, S9, S10 and commercial Cu particles increases to about 124%, slightly less than theoretical value (125%), suggesting the presence of trace oxygen species on the surface of S3, S9, S10 and commercial Cu. Figure 8b shows the H_2-TPR curves of porous Cu (S3, S9, and S10) and commercial Cu, as well as Cu_2O (S1) as reference. It is seen that a large H_2 consumption peak for Cu_2O (S1) is located at about 370 °C, whereas a very weak peak appears at about 280−400 °C for prepared Cu samples (S3, S9, and S10) and commercial Cu (inset of Figure 8b). The calculated amount of H_2 consumption for all Cu samples is about 1% of that of Cu_2O (S1), suggesting the presence of predominant metallic Cu for porous Cu samples (S3, S9, and S10) with trace oxygen species on their surface because their high surface area,[55] which is further confirmed by X-ray photoelectron spectroscopy analysis (not shown here).

Table 3 shows the catalytic performance of porous Cu (S3, S9, and S10) and commercial Cu as copper catalysts for Rochow reaction. It can be seen that porous Cu products exhibit higher Si conversions of 32.8% (S3), 31.5% (S9), and 33.5% (S10) at 325 °C, than that of the commercial Cu (15.0% at 325 °C). More importantly, the porous cubic Cu catalyst shows a higher M2 selectivity of 68.3% (S3), 67.5% (S9), and 67.3% (S10) at 325 °C, compared with that of the commercial Cu particles (55.0% at 325 °C). As M2 is the most valuable precursor in organosilane industry, the results demonstrate that the synthesized porous Cu exhibits much better catalytic activity for M2 synthesis and higher Si conversion. The porous Cu samples S3, S9, and S10 with a similar pore structure (their surface area is 5.7, 5.3, and 4.9 m^2/g, respectively) and particle size but different morphologies show a similar catalyst

dx.doi.org/10.1021/am3002605 | ACS Appl. Mater. Interfaces 2012, 4, 1295−1302

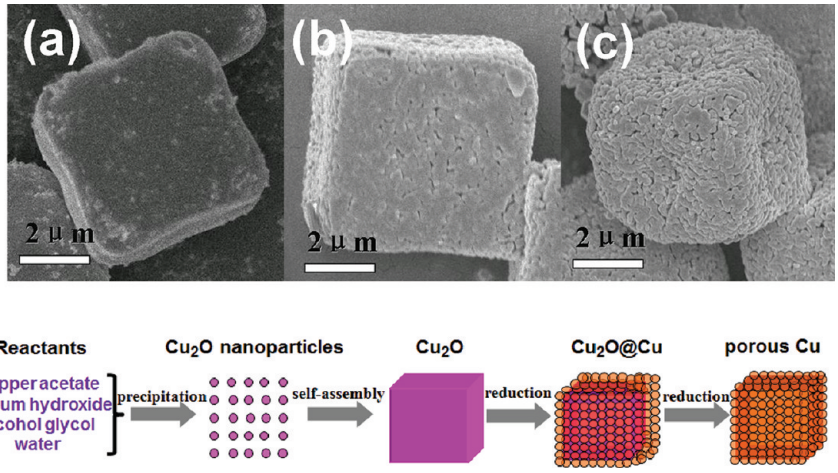

Figure 7. SEM images of samples obtained at (a) 3 h (S1), (b) 6 h (S2), (c) 10 h (S3), and (d) illustration of the possible formation process of porous cubic Cu.

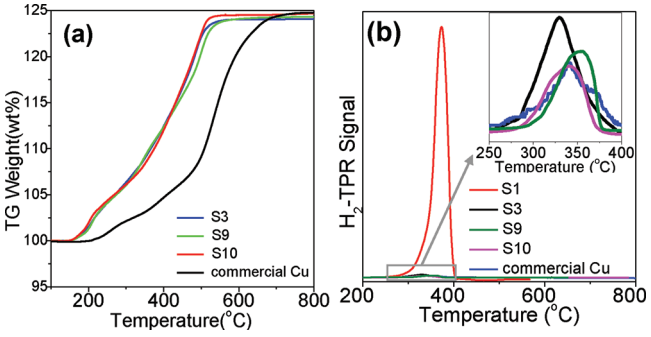

Figure 8. (a) TG curves of porous Cu samples (S3, S9, and S10) and commercial Cu in air, (b) H_2-TPR curves of Cu_2O (S1) and porous Cu samples (S3, S9, and S10), as well as commercial Cu.

Table 3. Catalytic Performance of Porous Cu Microparticles for Rochow Reaction

samples	S_{M1} (%)	S_{M2} (%)	S_{M3} (%)	C_{Si} (%)
S3	30.2	68.3	1.5	32.8
S9	31.1	67.5	1.4	31.5
S10	31.2	67.3	1.5	33.5
commercial Cu	48.2	55.0	1.8	15.0

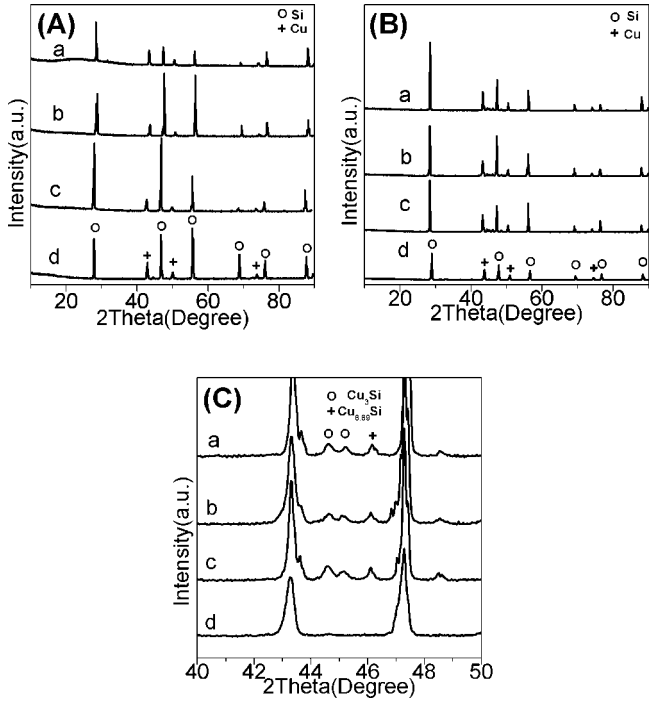

Figure 9. XRD patterns of contact masses (porous Cu and commercial Cu mixed with silicon) (A) before and (B) after reaction, and enlarged view of (B) in the range of 40−50° (C) (a, S3+Si; b, S9+Si; c, S10+Si; and d, commercial Cu+Si).

performance, implying the less influence of porous Cu morphology on the catalytic property.

Panels A and B in Figure 9 display XRD patterns of the contact mass before and after reaction, which was the solid mixture of the reactant Si, the catalyst Cu, and Zn as promoter. Prior to the reaction, all contact masses (Cu+Si) exhibit similar XRD patterns as shown in Figure 9A. After the reaction, Cu and Si species were detected in the spent contact masses as shown in Figure 9B. An enlarged view in the range of 40−50° (Figure 9C) shows the presence of Cu_3Si and $Cu_{6.69}Si$ species, suggesting the formation of alloyed Cu_xSi active components for all the synthesized samples. In Rochow reaction, Cu_3Si is normally suggested as the key catalytic active species,[56] on which M2 is produced.[57] Cu_3Si formed between copper catalyst and Si interface[58] is an indicator of the Cu catalyst activity.[59] When copper and silicon are brought together at elevated temperatures, Cu_3Si (eta phase) is formed.[60] It has been reported that MCSs can be produced from MeCl monolayers that were generated on Cu_3Si surfaces containing excess silicon.[59] The amount of Cu_3Si can substantially affect the Si conversion and M2 selectivity.[37] Although the intensity of Cu peaks for all the reacted contact masses are very similar, a much higher intensity of Cu_xSi is observed for the porous Cu than the commercial Cu, suggesting that the porous Cu is more active in generating Cu_xSi than the commercial Cu. The direct synthesis is considered as a kinetically determined reaction, driven by the choice of a catalyst and by the addition of certain promoters to an optimum between reactivity (reaction rate) and selectivity (yield) with respect to the desired main product M2. The pore structure within Cu particles could result in more contact areas between Si and Cu interface enhancing the formation of more Cu_xSi species and kinetically favor MeCl gas transportation for fast reaction, both of which could lead to the relatively high M2

dx.doi.org/10.1021/am3002605 | ACS Appl. Mater. Interfaces 2012, 4, 1295−1302

selectively and Si conversion compared to the nonporous Cu particles. We also found the shorter induction period for porous Cu particles compared to nonporous particles. More investigation is indeed demanded considering other factors.

Despite porous Cu microparticles synthesized in this work show a higher M2 selectivity and Si conversion than commercial dense Cu microparticles, it should be mentioned that their catalytic performance is much lower than that of commercial copper catalysts, e.g., Cu−Cu_2O−CuO.[61] This is because the commercial copper catalysts contains multiple copper components such as Cu, Cu_2O, and CuO, together with other promoters such as Sn and P,[62] which could increase the Si conversion and M2 selectivity. Our intension in this work is to only explore the pore effect of copper catalysts on catalytic property for Rochow reaction. Along this way, many nanostructured copper catalysts would be developed.

4. CONCLUSIONS

In conclusion, we have demonstrated a facile solvothermal method to prepare porous cubic Cu with a size in the range of 3−6 μm, depending on the synthesis conditions such as reaction time, temperature, and the reactant amounts. Compared with the commercial dense Cu microparticles, porous cubic Cu microparticles show better oxidability, much higher M2 selectivity, and Si conversion in Rochow reaction. This is due to the presence of porous structure that enhances the gas transportation and leads to the more Cu−Si contact area, thus forming much more active Cu_xSi. The work adds a new example of porous metal and would be helpful in developing novel porous copper catalysts and understanding the Rochow catalytic reaction mechanism.

AUTHOR INFORMATION

Corresponding Author

*E-mail: fbsu@mail.ipe.ac.cn, Tel.: +86-10-82544850, Fax: +86-10-82544851.

Notes

The authors declare no competing financial interest.

ACKNOWLEDGMENTS

The authors gratefully acknowledge the supports from the Hundred Talents Program of the Chinese Academy of Sciences (CAS), CAS-Locality Cooperation Program (DBNJ-2011-058), State Key Laboratory of Multiphase Complex Systems (MPCS-2011-D-14), National Natural Science Foundation of China (21031005), and China Postdoctoral Science Foundation (20110490597).

REFERENCES

(1) Lu, L.; Sui, M. L.; Lu, K. *Science* **2000**, *287*, 1463−1466.
(2) Sun, Y.; Xia, Y. *Science* **2002**, *298*, 2176−2179.
(3) Hakamada, M.; Mabuchi, M. *Nano Lett.* **2006**, *6*, 882−885.
(4) Liu, Y.; Walker, A. R. H. *Angew. Chem., Int. Ed.* **2010**, *49*, 6781−6785.
(5) Li, Z. Q.; Li, B. Q.; Qin, Z. X.; Lu, X. *J. Mater. Sci.* **2010**, *45*, 6494−6497.
(6) Hamby, D. C.; Hoover, N. J.; Wirkkala, J.; Zahnle, D. *J. Electrochem. Soc.* **1979**, *126*, 2110−2118.
(7) Jiao, Z. J.; Takagi, N.; Shikazono, N.; Kasagi, N. *J. Power Sources* **2011**, *196*, 1019−1029.
(8) Gloria, D.; Gooding, J. J.; Moran, G.; Hibbert, D. B. *J. Electroanal. Chem.* **2011**, *656*, 114−119.
(9) Jalem, R.; Koike, R.; Yang, Y.; Nakayama, M.; Nogami, M. *Nano Res.* **2011**, *4*, 746−758.
(10) Hu, C.; Gao, Z.; Yang, X. *J. Cryst. Growth* **2007**, *306*, 390−394.
(11) Fang, C.; Ellis, A. V.; Voelcker, N. H. *J. Electroanal. Chem.* **2011**, *659*, 151−160.
(12) Yang, Y.; Wu, Y. H.; Hao, P.; Zhang, Z. Q. *Spectrosc. Spect. Anal.* **2010**, *30*, 1898−1901.
(13) Zheng, R. B.; Guo, X. L.; Fu, H. *Appl. Surf. Sci.* **2011**, *257*, 2367−2370.
(14) Xue, L. G.; Fu, Z. H.; Yao, Y.; Huang, T.; Yu, A. S. *Electrochim. Acta* **2010**, *55*, 7310−7314.
(15) Xue, L. J.; Xu, Y. F.; Huang, L.; Ke, F. S.; He, Y.; Wang, Y. X.; Wei, G. Z.; Li, J. T.; Sun, S. G. *Electrochim. Acta* **2011**, *56*, 5979−5987.
(16) Ju, Y. W.; Eto, H.; Inagaki, T.; Ida, S.; Ishihara, T. *J. Power Sources* **2010**, *195*, 6294−6300.
(17) Magdassi, S.; Grouchko, M.; Kamyshny, A. *Materials* **2010**, *3*, 4626−4638.
(18) Molenbroek, A. M.; Haukka, S.; Clausen, B. S. *J. Phys. Chem. B* **1998**, *102*, 10680−10689.
(19) Ma, J.; Li, L.; Ren, J.; Li, R. *Sep. Purif. Technol.* **2010**, *76*, 89−93.
(20) Umamaheswari, V.; Hartmann, M.; Poppl, A. *J. Phys. Chem. B* **2005**, *109*, 1537−1546.
(21) Jeong, S.; Song, H. C.; Lee, W. W.; Lee, S. S.; Choi, Y.; Son, W.; Kim, E. D.; Paik, C. H.; Oh, S. H.; Ryu, B. H. *Langmuir* **2011**, *27*, 3144−3149.
(22) Shin, J.; Moon, H.; Kim, B.; Kim, K.; Lee, H.; Jung, S.; Kwon, H. *Curr. Appl Phys.* **2011**, *11*, S283−S288.
(23) Salzemann, C.; Brioude, A.; Pileni, M. P. *J. Phys. Chem. B* **2006**, *110*, 7208−7212.
(24) Rathmell, A. R.; Bergin, S. M.; Hua, Y. L.; Li, Z. Y.; Wiley, B. J. *Adv. Mater.* **2010**, *22*, 3558−3563.
(25) Salzemann, C.; Urban, J.; Lisiecki, I.; Pileni, M. P. *Adv. Funct. Mater.* **2005**, *15*, 1277−1284.
(26) Cao, Y.; Fan, J.; Bai, L.; Hu, P.; Yang, G.; Yuan, F.; Chen, Y. *Cryst. Growth Des.* **2010**, *12*, 3894−3899.
(27) Ni, Y.; Wang, B.; Liu, R.; Hong, J. *Cryst. Res. Technol.* **2009**, *44*, 1293−1296.
(28) Fu, J. X.; Wu, S.; Zhao, Y. P. *J. Phys. Chem. C* **2008**, *112*, 5459−5462.
(29) Yan, C.; Xue, D. *Cryst. Growth Des.* **2008**, *8*, 1849−1854.
(30) Zhang, Y.; Xing, R.; Yahu, X. *Cryst. Growth Des.* **2004**, *273*, 280−284.
(31) Ren, X.; Chen, D.; Tang, F. *J. Phys. Chem. B* **2005**, *109*, 15803−15807.
(32) Liu, Y.; Chu, Y.; Zhuo, Y.; Dong, L.; Li, L.; Li, M. *Adv. Funct. Mater.* **2007**, *17*, 933−938.
(33) Kondoh, E.; Fukuda, J. *J. Supercrit. Fluids* **2008**, *44*, 466−474.
(34) Rochow, E. G. *J. Am. Chem. Soc.* **1945**, *67*, 963−965.
(35) Acker, J.; Bohmhammel, K. *J. Organomet. Chem.* **2008**, *693*, 2483−2493.
(36) Zhang, Z.; Che, H.; Wang, Y.; Gao, J.; Zhao, L.; She, X.; Sun, J.; Gunawan, P.; Zhong, Z.; Su, F. *Ind. Eng. Chem. Res.* **2012**, *51*, 1264−1274.
(37) Lewis, L. N.; Ward, W. J. *Ind. Eng. Chem. Res.* **2002**, *41*, 397−402.
(38) Zhang, Z.; Che, H.; Wang, Y.; Gao, J.; She, X.; Sun, J.; Zhong, Z.; Su, F. *RSC Adv.* **2012**, *2*, 2254−2256.
(39) Barr, M. K.; Murphy, T. M.; Williams, M. G. USP-20050176981, 2005.
(40) Voorhoeve, R.; Geertsem, B.; Vlugter, J. C. *J. Catal.* **1965**, *4*, 43−47.
(41) Bablin, J. M.; Crawford, A. C.; DeMoulpied, D. C.; Lewis, L. N. *Ind. Eng. Chem. Res.* **2003**, *42*, 3555−3565.
(42) Luo, W.; Wang, G.; Wang, J. *Ind. Eng. Chem. Res.* **2006**, *45*, 129−133.
(43) Wu, Z. J.; Zhao, J. S.; Zhang, M. H.; Li, W.; Tao, K. Y. *Catal. Commun.* **2010**, *11*, 973−976.
(44) Zhang, X. J.; Wang, G. F.; Wu, H. B.; Zhang, D.; Zhang, X. Q.; Li, P.; Wu, H. Q. *Mater. Lett.* **2008**, *62*, 4363−4365.

(45) Liang, D. D.; Liu, S. X.; Ma, F. J.; Wei, F.; Chen, Y. G. *Adv. Synth. Catal.* **2011**, *353*, 733−742.
(46) Salavati-Niasari, M.; Davar, F.; Mir, N. *Polyhedron* **2008**, *27*, 3514−3518.
(47) Jenkins, R.; Snyder, R. L. *Introduction to X-ray Powder Diffractometry* **1996**, *248*, 89−91.
(48) Brunauer, S.; Emmett, P. H.; Teller, E. *J. Am. Chem. Soc.* **1938**, *60*, 309−319.
(49) Barrett, E. P.; Joyner, L. G.; Halenda, P. P. *J. Am. Chem. Soc.* **1951**, *73*, 373−380.
(50) Lyons, C. P. H.; Roussillon, G. S. USP-4661613, 1987.
(51) Sun, J.; Jing, Y.; Jia, Y. Z.; Tillard, M.; Belin, C. *Mater. Lett.* **2005**, *59*, 3933−3936.
(52) Bradbury, A. J.; Lincoln, S. F.; Wainwright, K. P. *J. Inclusion Phenom. Macrocyclic Chem.* **2011**, *71*, 567−575.
(53) Wu, C. Y.; Yu, S. H.; Antonietti, M. *Chem. Mater.* **2006**, *18*, 3599−3601.
(54) Shen, Y. H.; Li, S. K.; Li, C. H.; Huang, F. Z.; Wang, Y.; Xie, A. J.; Wu, Q. *J. Nanopart. Res.* **2011**, *13*, 2865−2874.
(55) Guo, H. Q.; Li, D. B.; Jiang, D.; Xiao, H. C.; Li, W. H.; Sun, Y. H. *Catal. Today* **2010**, *158*, 439−445.
(56) Banholzer, W. F.; Burrell, M. C. *J. Catal.* **1988**, *114*, 259−270.
(57) Frank, T. C.; Kester, K. B.; Falconer, J. L. *J. Catal.* **1985**, *91*, 44−53.
(58) Banholzer, W. F.; Lewis, N.; Ward, W. *J. Catal.* **1986**, *101*, 405−415.
(59) Sun, D.; Bent, B. E. *Catal. Lett.* **1997**, *46*, 127−132.
(60) Stolt, L.; Heurle, D. F. M. *Thin Solid Films* **1990**, *189*, 269−274.
(61) Lewis, K. M.; Ritscher, J. S. USP-7153991, 2006.
(62) Gordon, A. D.; Hinch, B. J.; Strongin, D. R. *Catal. Lett.* **2009**, *133*, 14−22.